



Wedge splitting test method: quantification of influence of glued marble plates by two-parameter fracture mechanics

S. Seitl

Academy of Sciences of the Czech Republic, v. v. i., Institute of Physics of Materials, Brno, Czech Republic and Brno University of Technology, Faculty of Civil Engineering, Institute of Structural Mechanics, Brno, Czech Republic
seitl@ipm.cz

B. Nieto García

Academy of Sciences of the Czech Republic, v. v. i., Institute of Physics of Materials, Brno, Czech Republic and University of Oviedo, Department of Construction and Manufacturing Engineering Campus de Viesques, Gijón, Spain
UO209943@uniovi.es

I. Merta

University of Technology Vienna, Faculty of Civil Engineering, Institute of Building Construction and Technology, Vienna, Austria
ildiko.merta@tuwien.ac.at

ABSTRACT. In the present paper, the well-known wedge splitting test (WST) is applied on specimens with different geometries ($S=150, 200, 300$ mm) and variants of the specimens' configurations. K-calibration (B_1) and T-stress (B_2) calibration curves for such specimens are introduced. The objective was to compare and discuss the values of the calibration curves dependent on the specimen's geometries and on three different specimens' configurations: homogenous specimen; specimen with marble plates forming the groove for load application and specimen with glued marble plates.

KEYWORDS. Wedge splitting test; Stress intensity factor, T-stress; K-calibration curves; Concrete fracture test.

INTRODUCTION

The wedge splitting test (WST) is nowadays a popular test for measuring fracture properties of materials like concrete [7, 17, 18, 24]. The WST was developed by Linsbauer and Tschegg [22] and patented by Tschegg in 1986 [30]. A modified WST with different wedge equipment was published by Bruhwiler and Wittmann in 1990 [5]. It is a very stable test for determining the fracture energy of concrete. The specimens used are very compact and require small amounts of material compared to the notched beams employed in three-point bending tests (3PBT). However, the implementation of this type of test requires more sophisticated tools than the 3PBT and the number of experimental results available in the literature obtained using the WST of concrete is very limited. Calibration curves for the WST are not as widely reported. Stress intensity factors (SIF, K-factor) for particular variants of the WST (cube-shaped specimens) can be found in the literature, e.g. Guinea et al. [10]. K and T-stress calibration curves for foam concrete with marble plates forming the rectangular groove on the upper side of WST specimens are presented in [29]. Multi-parameter

description of stress and displacement fields by means of the Williams power series using also higher-order terms for homogenous specimens can be found in Malíková and Veselý [23]. Coefficients of this series are determined via the over-deterministic method from the results of conventional finite element (FE) analysis. The lattice modeling of WST can be found in Frantík et al. [9].

In the WST for the assembly of the load transmission pieces and of the wedge, a rectangular groove is needed on the upper side of the specimens. There are generally three ways (with their advantages and disadvantages) for preparation of the rectangular groove. According to the literature, the most traditional way is to cut this part out of the specimens with a diamond saw; see e.g. [7, 30]. However, this is a very time consuming and demanding procedure.

Another method is to form the groove in the specimens by placing a rectangular bar into the standard cube moulds when casting the specimens. In the paper by Korte et al. [17, 18], the bar was attached to the side of the mould in order to obtain a plain top surface of the groove. The authors Kim and Kim used the 10-mm groove to insert the triangular prism at each outer side. Here, the initial notch was made by inserting a steel plate into the specimens during the casting and the plate was taken out after one day. The use of special moulds to produce notch and grooves in mortar samples has been widely reported [28]. However, this method is generally applicable for concretes with small aggregate size. When working with concretes of larger aggregate size the bars placed into the mould during the casting could have a significant influence on the distribution of the particles in the matrix resulting in non-realistic results of the experiments.

The most convenient and easiest way to obtain the rectangular groove is to form it by gluing two marble plates on the upper side of the specimens, see [24]. First, a thin layer of the specimens should be cut off the top in order to obtain a completely plane surface and then the starter notch should be cut. The marble plates are then glued to the specimens with two-component glue.

In this paper the parametrical study of the WST within the framework of two-parameter fracture mechanics is applied for the case where the rectangular groove on the upper side of the specimens was formed by gluing two marble pieces thereon and for the case where the rectangular groove was obtained by cutting it out from the specimens. The stress intensity factor calibration curves and the T-stress calibration curves are determined and compared among three variants of the WST configuration: i) homogenous specimen, ii) specimen where the rectangular groove is formed by two marble plates without glue (see Fig. 1a) and iii) specimen with a glue layer between marble plates and concrete (see Fig. 1b). Note that in composite structures and materials, the weakest part is often the interface between different materials. Note also that the fracture mechanics parameters of materials are important data for numerical calculation during the structural design [13,14,26,27]

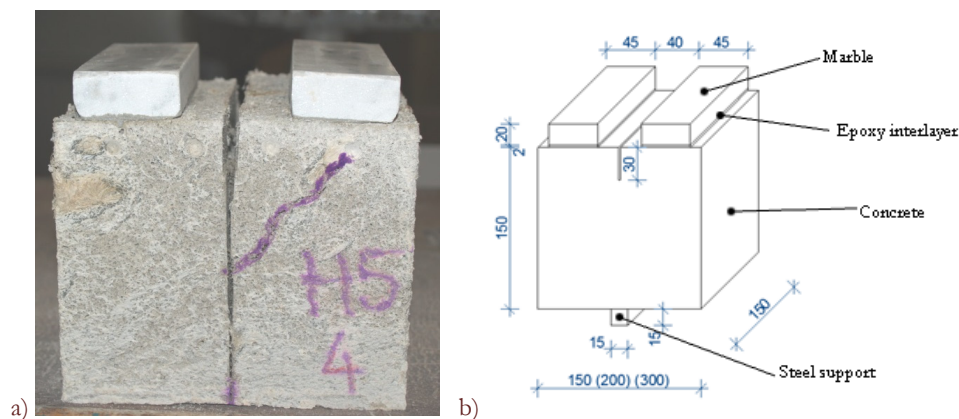


Figure 1: Wedge splitting specimen: a) photo and b) sketch: where the rectangular groove is formed by two marble plates glued on the upper side of the specimen.

THEORETICAL BACKGROUND

According to the two-parameter fracture mechanics approach which uses T-stress as a constraint parameter [1,2,29,32], the stress field around the crack-tip of a two-dimensional crack embedded in an isotropic linear elastic body subjected to normal mode I loading conditions is given by the following expressions by Williams [31]:



$$\begin{aligned} \sigma_{xx} &= \frac{K_I}{\sqrt{2\pi r}} \cos\left(\frac{\theta}{2}\right) \left[1 - \sin\left(\frac{\theta}{2}\right) \sin\left(\frac{3\theta}{2}\right) \right] + T & (a) \\ \sigma_{yy} &= \frac{K_I}{\sqrt{2\pi r}} \cos\left(\frac{\theta}{2}\right) \left[1 + \sin\left(\frac{\theta}{2}\right) \sin\left(\frac{3\theta}{2}\right) \right] & (b) \\ \tau_{xy} &= \frac{K_I}{\sqrt{2\pi r}} \cos\left(\frac{\theta}{2}\right) \sin\left(\frac{\theta}{2}\right) \cos\left(\frac{3\theta}{2}\right) & (c) \end{aligned} \quad (1)$$

where r and θ are the polar coordinates and x and y are the Cartesian coordinates, both with their origins at the crack tip. K_I is the stress intensity factor for mode I and T is the T -stress. Thus, in two-parameter based fracture mechanics, the stress field is expressed by means of these two parameters, the stress intensity factor K_I and the T -stress (see e.g. [2]). According to Leevers and Radon [20] the SIF and the T -stress may be normalized for the testing geometries in question to be dimensionless as follows:

$$B_1 = \frac{K_I}{K_0}, \quad \text{where} \quad K_0 = \frac{P_{sp}}{t\sqrt{W}} \quad (2)$$

and

$$B_2 = \frac{T\sqrt{\pi a}}{K_I} \quad (3)$$

where P_{sp} is the horizontal component of the loading (the splitting force), t is the specimen thickness, W is the fundamental specimen dimension (specimen size) and a represents the crack length.

INPUT MATERIAL PARAMETERS

In order to obtain the relevant calibration curves, a literature overview [4] of materials properties was conducted. The range of real materials properties are summarized in Tab. 1. On the basis of this data the theoretically possible intervals of properties (Young's modulus and Poisson's ratio) for particular materials were selected as follow: The values of marble are $E \in <10; 100>$ GPa and $\nu = 0.3$, the values of epoxy in layer are $E = 5$ GPa and $\nu = 0.4$, the values of concrete are $E \in <1; 100>$ GPa and $\nu = 0.2$ and for steel parts the traditional values are used $E = 210$ GPa and $\nu = 0.3$.

Materials/Elastic materials property	Young's modulus [GPa]	Poisson ratio [1]
Marble in [8]		
Georgia marble	23.4÷42.1	-
Tennessee marble	53.1÷76.5	-
Russian marble	9.0÷20.7	-
Marble in [16]	91.7	-
Marble in [11]	-	0.2-0.3
Epoxy inlayer in [6]	1÷5	0.35÷0.43
Concrete in [3]	30.6÷33.22	0.18÷0.21
Foam concrete [12]	1÷8	-
High performance self-compacting concrete in [33]	30÷50	-
High performance concrete in [25]	58÷62	0.02÷0.2
Lightweight concrete in [19]	10.39÷35.92	0.2
Ultra high performance concrete [15]	50÷75	-
Ultra high performance concrete in [21]	95÷100	-

Table 1: Information of selected material properties.

NUMERICAL SIMULATION

For numerical calculations of both boundary conditions the characteristic dimension, 150 mm (marked in the text as W), was used, see Fig. 1. The values of forces during the numerical simulation are follow in splitting direction (axe y) is $P_{sp} = 1000$ N and the vertical load (axe x) is $P_v = 535.89$ N according the equation:

$$P_v = \frac{1}{2} P_{sp} k \quad (4)$$

where

$$k = \frac{2 \tan \alpha_w + \mu_c}{1 - \mu_c \tan \alpha_w} \quad (5)$$

The symbol α_w represents the angle of the wedge ($\alpha_w = 15^\circ$, according to [24]) and μ_c refers to friction in the roller bearings. Note that the influence of friction was studied in [29] and is not the subject of this study.

The selected numerical model with boundary conditions is shown in Fig 2. The interfaces between materials were modeled as ideal adhesion (for both materials the same displacement and deformation values in transition nodes were used). The initiation notch length was modeled as a crack (i.e. of zero width). The material input data for the concrete, marble and glue layer used in the numerical simulation are mentioned in paragraph input material parameters. The stress intensity factor K and the T-stress values were computed using the direct method [32] and after that normalized according eqs. (2) and (3).

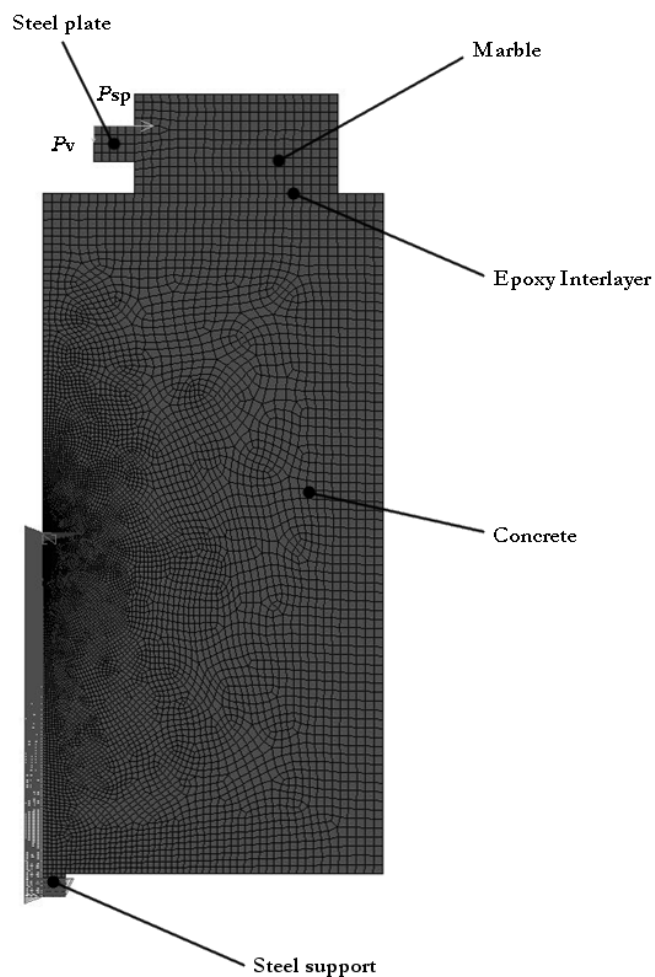


Figure 2: Numerical model of wedge splitting specimens with boundary conditions, symmetrical half.



RESULTS AND DISCUSSION

The numerically calculated values of the normalized SIF (i.e. B_1) and T-stress (i.e. B_2) are plotted in Figs. 3 and 4, respectively. In the present paper, two issues of the specimens' shapes/arrangements on the calibration curves were investigated: i) the influence of the material inhomogeneity of specimens, i.e. the homogeneous variant, the variant with marble parts and ii) the variant with marble parts glued by epoxy and change of length $S = 150, 200$ and 300 mm.

The change of the WST specimen lengths

In Fig. 3 the dependencies of B_1 as a function of ratio α has been plotted. The dependencies show practically the same trends, the functions of calibration curve for $S = 150, 200$ and 300 mm can be introduced as follows:

$$B_1(150) = 11928 \alpha^6 - 30294 \alpha^5 + 30425 \alpha^4 - 15149 \alpha^3 + 3881.4 \alpha^2 - 462 \alpha + 24.573 \quad (6)$$

$$B_1(200) = 11940 \alpha^6 - 30409 \alpha^5 + 30644 \alpha^4 - 15319 \alpha^3 + 3951 \alpha^2 - 447.98 \alpha + 24.97 \quad (7)$$

$$B_1(300) = 11947 \alpha^6 - 30414 \alpha^5 + 30626 \alpha^4 - 15295 \alpha^3 + 3942.7 \alpha^2 - 4.77.98 \alpha + 24.889 \quad (8)$$

All three studied cases, except for length S , are for the rest of geometrical aspects similar and so similar values of the normalized stress intensity factor B_1 were expected. This fact is obvious especially for long cracks ($\alpha > 0.6$), where the influence of the length on the stress state around the crack tip can be supposed to vanish.

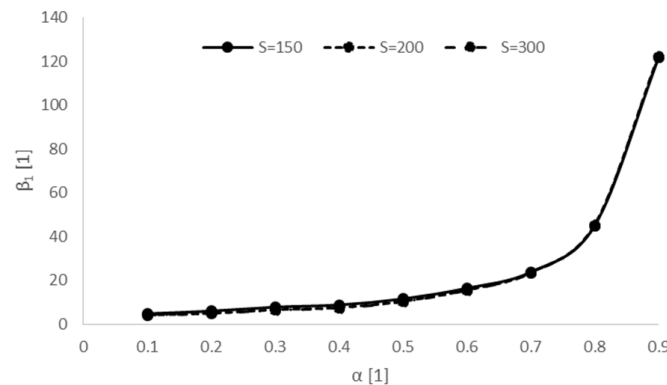


Figure 3: The values of normalized stress intensity factor B_1 for three cases of homogeneous concrete specimens of lengths $S = 150, 200, 300$ mm.

The normalized T-stress values expressed in Fig. 4 as the $B_2(\alpha)$ functions vary from negative values for very short cracks to positive values for relative crack lengths larger than approximately 0.15 in all studied cases.

$$B_2(150) = 8.7758 \alpha^6 + 20.471 \alpha^5 - 56.862 \alpha^4 + 43.872 \alpha^3 - 20.216 \alpha^2 + 7.9127 \alpha - 0.7082 \quad (9)$$

$$B_2(200) = 49.463 \alpha^6 - 101.89 \alpha^5 + 70.194 \alpha^4 - 6.3491 \alpha^3 - 14.923 \alpha^2 + 7.4399 \alpha - 0.6945 \quad (10)$$

$$B_2(300) = 83.718 \alpha^6 - 200.77 \alpha^5 + 172.51 \alpha^4 - 50.561 \alpha^3 - 7.8443 \alpha^2 + 6.9177 \alpha - 0.6806 \quad (11)$$

Values of $B_2(\alpha)$ for all three geometries tend to be equal for very long cracks only ($\alpha > 0.85$).

Influence of material inhomogeneity

In this study, the influence of the WST specimen composition on the near-crack tip stress field fracture parameters was investigated (WST specimen is made from: i) concrete, ii) concrete and marble iii) concrete, marble and epoxy). According to the paragraph Input Materials Parameters, the various combinations of materials properties for selected part of WST were used.



The B_1 and B_2 as a function of α has practically the same values for all cases, see Fig. 5a and 5b, and the same calibration curve can be used for all three cases. This means that neither the use of marble parts nor the epoxy layer has an influence on the calibration curve.

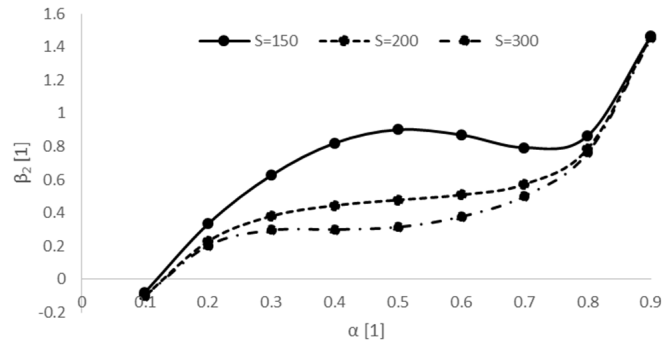


Figure 4: The values of normalized stress intensity factor B_2 for three cases of homogeneous concrete specimens of lengths $S = 150, 200, 300$ mm

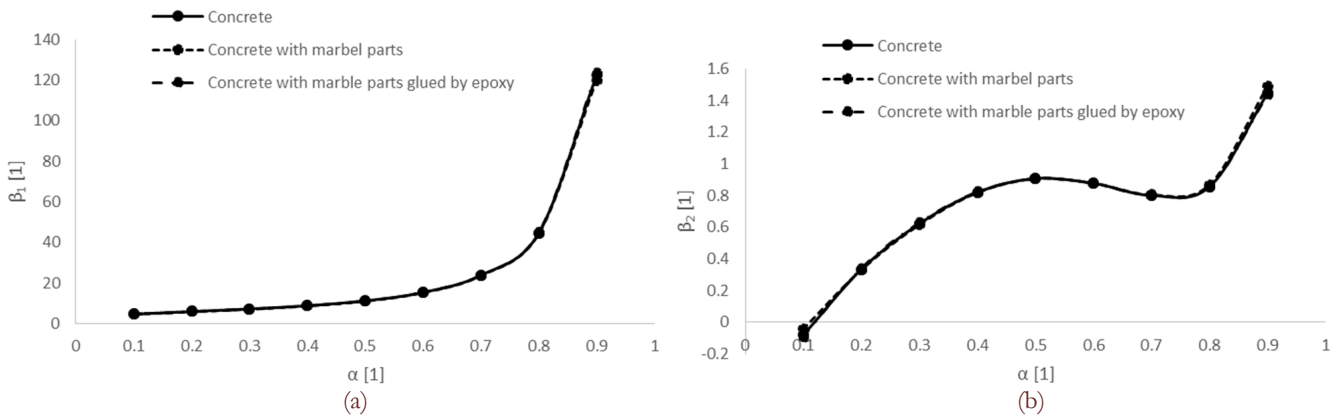


Figure 5: The values of normalized stress intensity factor B_1 and T -stress B_2 for $W = 150$ mm for three cases: i) concrete ($E = 40$ GPa), ii) concrete ($E = 1$ GPa) with marble parts ($E = 100$ GPa) and iii) concrete ($E = 100$ GPa) with marble parts ($E = 10$ GPa) glued by epoxy ($E = 5$ GPa).

For quantification of the error caused by the various kinds of material the graphs of maximal deviation between the homogeneous specimen and with marble and epoxy part are plotted in Fig. 6. In Fig. 6, these show the maximal percentual difference for $0.3 \leq \alpha \leq 0.8$. The error is smaller than 1.5 % and it is possible to neglect it in the evaluation of fracture parameters (fracture energy, etc...). Therefore, the polynomial approximations dependence on the length of specimen for both B_1 and B_2 can be used.

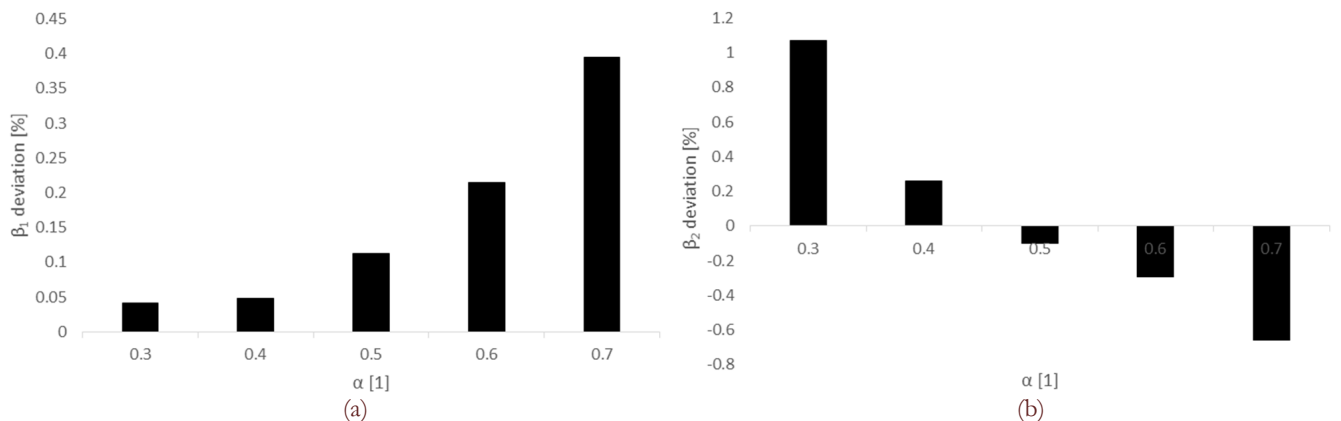


Figure 6: The maximal percentual difference for various WST specimen compositions: a) for biaxial parameter B_1 and b) for biaxial parameter B_2 .



CONCLUSIONS

A finite element analysis of the wedge splitting test on specimens modified by replacement of the load transmitting parts with a stiffer material was performed by means of a constraint-based two parameter fracture mechanics approach.

The study focused on two aspects:

- Investigation of the influence of the length of the WST specimens (150, 200 and 300 mm)
- Investigation of the influence of the specimens' inhomogeneity (different concrete, different marble, epoxy layer and steel)

The principal conclusions derived from this work are the following:

- The influence of the specimens' length on the calibration curves values is not negligible and for each case a different polynomial function has to be used, see Fig. and Eq. (6-11).
- The influence of the specimens' inhomogeneity on the calibration curves' values is negligible and the same polynomial function covers all cases, see Fig. 5 and the possible mistake/deviation of results are smaller than 1.5 %.

ACKNOWLEDGEMENTS

The investigation reported in this paper was supported by grants No. 7AMB1 4AT012, CZ. 107/2.3.00/20.0197 and FAST-S-14-2532.

REFERENCES

- [1] Aliha, M.R.M., Ayatollahi, M.R., Two-parameter fracture analysis of SCB rock specimen under mixed mode loading, *Engineering Fracture mechanics*, 103 (2013) 115–123.
- [2] Anderson, T. L., *Fracture mechanics: Fundamentals and applications*. New York, CRC Press LLC, (1995) 688.
- [3] Bahr, O., Schaumann, P., Bollen, B., Bracke, J. Young's modulus and Poisson's ratio of concrete at high temperatures: Experimental investigations, *Materials and Design*, 45 (2013) 421–429.
- [4] Boresi, A. P., Schmidt, R. J., Sidebottom, O. M. *Advanced Mechanics of Materials*, Wiley, (1993).
- [5] Bruhwiler E., Wittmann FH. The wedge splitting test: a new method of performing stable fracture mechanics tests, *Eng Fract Mech*, 35 (1990) 117–125.
- [6] Cease, H., Derwent, P.F., Diehl, H.T., Fast, J., Finley, D., Measurement of mechanical properties of three epoxy adhesives at cryogenic temperatures for CCD construction, *Fermilab/TM/2366 A*, (2006) 1–9.
- [7] Cifuentes, H., Karihaloo, B., Determination of size/independent specific fracture energy of normal- and high-strength self/compacting concrete from wedge splitting tests, *Construction and Buildings Materials*, 48(2013) 548–553.
- [8] Exadaktylos, G.E., Vardoulakis, I., Kourkoulis, S.K. Influence of nonlinearity and double elasticity on flexure of rock beams- I. Technical theory, *International Journal of Solids and Structures*, 38 (2001) 4091–4117.
- [9] Frantík, P., Veselý, V., Keršner, Z. Parallelization of lattice modelling for estimation of fracture process zone extent in cementitious composites, *Advances in Engineering Software*, 60-61 (2013) 48–57.
- [10] Guinea, G.V., Elices, M., Planas J. Stress intensity factors for wedge-splitting geometry, *Int J Fracture*, 81 (1996) 113–124
- [11] http://www.engineeringtoolbox.com/poissons-ratio-d_1224.html.
- [12] Jones, M.R., McCarthy, A., Preliminary views on the potential of foamed concrete as a structural material, *Mag Concr Res*, 57 (2005) 21–31.
- [13] Katzer, J., Domski, J., Optimization of fibre reinforcement for waste aggregate cement composite, *Construction and Building Materials*, 38 (2013) 790–795.
- [14] Kim J., Kim Y., Fatigue crack growth of high-strength concrete in wedge-splitting test, *Cement and Concrete Research*, 29 (1999) 705–712.
- [15] Kimbauer, J., Vacuum Mixing of Ultra High Performance Concrete, Doctoral Thesis, Vienna University of Technology, Faculty of Civil Engineering, (2013).



- [16] Koca, M.Y., Ozden, G., Yavuz, A.B., Kincal, C., Onargan, T., Kucuk, K., Changes in the engineering properties of marble in fire-exposed columns, *International Journal of Rock Mechanics & Mining Sciences*, 43 (2006) 520–530.
- [17] Korte, S., Boel, V., De Corte, W., De Schutter, G., Static and fatigue fracture mechanics properties of self-compacting concrete using three-point bending tests and wedge-splitting tests, *Construction and Buildings Materials*, 57 (2014) 1–8.
- [18] Korte, S., Boel, V., De Corte, W., De Schutter, G., Vibrated concrete vs. self-compacting concrete: Comparison of fracture mechanics properties, *Key Engineering Materials*, 601 (2014) 199–202.
- [19] Kurugöl, S., Tanacan, L., Ersoy, H.Y., Young's modulus of fiber-reinforced and polymer-modified lightweight concrete composites, *Construction and Building Materials*, 22 (2008) 1019–1028.
- [20] Leever, P.S. Radon, J.C. Inherent stress biaxiality in various fracture specimen geometries, *International Journal of Fracture*, 19 (1983) 311–325.
- [21] Leutbecher, T., Rissbildung und Zugtragverhalten von mit Stabstahl und Fasern bewehrtem ultrahochfesten Beton (UHPC). Kassel: Kastel University Press, (2008).
- [22] Linsbauer H.N., Tschegg, E.K., Fracture energy determination of concrete with cube-shaped specimens, *Zement und Beton*, 31 (1986) 38–40.
- [23] Malíková, L., Veselý, V., The influence of higher order terms of Williams series on a more accurate description of stress fields around the crack tip, *Fatigue and Fracture of Engineering Materials and Structure*, (2014). doi: 10.1111/ffe.12221
- [24] Merta, I., Tschegg, E.K., Fracture energy of natural fibre reinforced concrete, *Construction and Building Materials*, 40 (2013) 991–997
- [25] Persson, B., Poisson's ratio of high-performance concrete, *Cement and Concrete Research*, 29(1999) 1647–1653.
- [26] Pryl, D., Červenka, J., Pukl, R., Material model for finite element modelling of fatigue crack growth in concrete. *Procedia Engineering*, 2 (2010) 203–212.
- [27] Pryl, D., Mikolaskova, J., Pukl, R., Modeling fatigue damage of concrete, *Key Engineering Materials*, 577–578 (2014) 385–388.
- [28] Ribeiro, S., De Campos Ribeiro, D., de Souza Dias, M.B., Ribeiro Garcia, G.C., Bento dos Santos, É.M., Study of the fracture behavior of mortar and concretes with crushed rock or pebble aggregates, *Mat. Res. São Carlos*, 14(1) (2011).
- [29] Seitl, S., Veselý, V., Routil, L. Two-parameter fracture mechanical analysis of a near-crack-tip stress field in wedge splitting test specimens, *Computers and Structures*, 89 (2001) 1852–1858.
- [30] Tschegg, E., Republik Österreich. Patent number 390328B, (1986).
- [31] Williams, M.L., On the stress distribution at the base of a stationary crack, *J Appl Mech*, 24 (1957) 109–14.
- [32] Yang, B., Ravi-Chandar, K., Evaluation of elastic T-stress by the stress difference method, *Engineering Fracture Mechanics*, 64 (1999) 589–605.
- [33] Yurtdas, I., Burlion, N., Shao, J.F. Li, A. Evolution of the mechanical behaviour of a high performance self-compacting concrete under drying, *Cement & Concrete Composites*, 33(2011) 380–388.